

Additive manufacturing of hybrid sandwich sheets by laser powder bed fusion of metals

S. Platt*, N. Schnell*, G. Witt*, S. Kleszczynski*†

**Institute for Product Engineering, University Duisburg–Essen, Lotharstr. 1, 47057
Duisburg, Germany*

†*Center for Nanointegration Duisburg- Essen (CENIDE), Carl-Benz-Str. 199, 47057
Duisburg, Germany*

Abstract

In the context of lightweight applications, laser powder bed fusion of metals allows the creation of high-complexity structures at minimal use of material. Traditional elements of lightweight construction are sandwich sheets, which comprise two cover sheets with a fine core structure joined in the centre. Thus, these lightweight elements contain both geometrically simple (cover sheets) and geometrically complex (core structure) elements. Conventional manufacturing of core structures is limited in terms of geometrical freedom. On the other hand, Additive Manufacturing of sheets has disadvantages in terms of economic efficiency. Therefore, a combined process consisting of additive and conventional cost-efficient manufacturing is proposed to eliminate both disadvantages. This publication presents a hybrid manufacturing route to produce metal sandwich sheets. The hybrid sandwich sheets are manufactured using a rolled cover sheet as a base plate and additive manufactured core structures including an upper cover sheet. For this purpose, a recently developed sheet mounting system for implementation in a laser powder bed fusion process is presented and evaluated concerning manufacturing criteria such as process stability and dimensional accuracy of the final components.

Introduction

Additive manufacturing (AM) is gaining acceptance in industry and research. Several AM processes are entering various industries and can provide a serious alternative to existing manufacturing processes. However, conventional production methods are in most cases more efficient in terms of mass production or cost-effective production chains. A combination of both, conventional and additive methods may therefore enable the avoidance of respective restrictions and the creation of synergistic effects. A promising application for this combination are sandwich sheets. Sandwich sheets offer a high potential for lightweight applications, such as in aircraft construction, aerospace, and the automotive industry. Further benefits may arise due to the optimal use of the material, the geometric freedom, and the possibility of integrating additional functionalities. [1]

In both, purely additive and conventional manufacturing, the production of sandwich sheets currently faces challenges such as poor material utilization or long production times. In the field of AM hybrid parts, most efforts focus on fabrication based on pre-milled blanks or the realization of functionally graded materials. Yin et al. [2] demonstrated a hybrid manufacturing technology combining laser powder bed fusion of metals (PBF-LB/M) and cold spraying to fabricate multi-material parts of Al/Al+Al₂O₃ and Ti6Al4V. Here, Al and Al+Al₂O₃ were cold sprayed on PBF-LB/M manufactured Ti6Al4V parts resulting in dense and machinable functionally graded materials. Although the PBF-LB/M Ti6Al4V section was represented by large pores and the cold sprayed section by small pores caused by insufficient particle plastic deformation. Tan et al. [3] investigated the interfacial characteristics and mechanical performance of steel-copper parts fabricated by PBF-LB/M. By applying appropriate laser parameters, a metallurgical bonded and dense steel-copper bi-metal was created. According to the authors, the high thermal conductivity of copper led to high Marangoni convection in the interface of the materials, which in turn led to excellent bonding.

The process concept of AM on metal sheets was already discussed in [4–8]. Ahuja et al. [5] presented a clamping concept that enabled PBF-LB/M on pre-formed metal sheets inside an SLM 280 HL machine. The mounting of the formed sheet was realized through a combination of a punch and clamping plate, which allowed the build-up on sheets with a thickness of 1.5 mm. The authors described the significant influence of an uneven sheet surface on the resulting shear strength of the hybrid components. Due to the uneven surface, an inhomogeneous powder distribution can occur on the metal sheet, which leads to insufficient bonding at the interface. Although implying great potential regarding lightweight applications, the build-up of sandwich structures on thin sheets of less than 1 mm has not yet been investigated.

In Rosenthal et. al [9], a new process combination route for AM sandwich sheets has been demonstrated. This work describes the AM process of sandwich sheets and their subsequent forming.

As a further approach, this contribution will examine the additive build-up of sandwich sheets based on rolled sheets of high formability to develop an alternative process route that combines the high formability of rolled steel sheets with the geometric freedom of AM. To consider the lightweight aspect of sandwich sheets, we demonstrate the additive build-up on sheet thicknesses of 0.5 mm.

Materials and Methods

Within this work, 17-4 PH stainless steel powder by eos GmbH was used. Furthermore, rolled DC01 (Fe_{99.19}Mn_{0.6} C_{0.12} P_{0.045} S_{0.045}) sheets with a thickness of 0.5 mm were applied as a base for the additive build-up. PBF-LB/M processing of the hybrid sandwich sheets was performed using an M270 system by eos GmbH, equipped with a 200 W Yb-fibre Laser ($\lambda = 1064$ nm). The utilized parameter sets, all as chessboard strategy, are shown in Table 1. The reference parameter (Ref) is the exposure parameter recommended by the machine manufacturer with a square size of 2 mm, as short scan vector lengths can lead to reduced thermal stress [10,11]. The purpose of the Ev- parameter was to reduce the temperature level that reaches the rolled sheet. Therefore, the square size was increased from 2 mm to 5 mm according to [12] to reduce the resulting temperature. Furthermore, it has already been shown in [13–15] that a reduction of the energy input can also reduce the residual stresses. Especially a reduction of the laser power causes a beneficial decrease in the occurring residual forces [16]. Therefore, the parameter set Ev- with a reduced volume energy density of approx. 54 % was selected. Whereby the main part of the reduced energy is achieved by doubling the layer thickness and reducing the laser power by 70 W (-36 %). The line energies of the parameters are comparable resulting in a relative density above 99 % which is comparable to [17–19].

Table 1: Exposure parameters used in the investigations

	Ref	Ev-
laser power [W]	195	125
scan speed [mm/s]	1000	700
layer thickness [mm]	0.02	0.04
volume energy density [J/mm ³]	108.33	49.60
square size [mm]	2	5

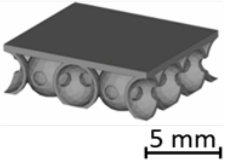
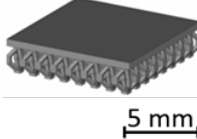
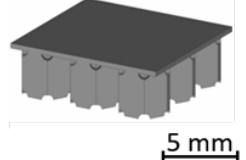
All experiments were executed under a nitrogen atmosphere and for all parameter sets a hatch distance of 0.09 mm was used. Furthermore, the scan vectors were rotated in 67° steps for each layer.

The build-up geometries are characterised in Table 2. The geometries are different structures of classical lightweight construction elements, but all with a thickness of the upper cover sheet of 0.3 mm. One selected structure is the honeycomb geometry (HC). The cross-sectional area

is divided into uniform hexagonal honeycombs with a constant wall thickness of 0.18 mm. At the upper and lower end of the core geometry, holes are provided to remove the loose powder. A framework (FW) was chosen as a further core structure. The design of the geometry is x-shaped, with each element being three-dimensional. In the centre is a cross-sectional area, from which four struts extend upwards and downwards, each with a lateral offset. The single struts have a nominal thickness of 0.25 mm. The connection points are made up of four bars and therefore have a thickness of 0.5 mm. Compared to the other geometries, the overall height is considerably lower at 2.48 mm.

Another core geometry used is the HDP geometry. This abbreviation can be derived from the theory of the hexagonal crystal system and stands for a hexagonal densely packed lattice. The three-dimensional spheres of the same size are each connected to the surrounding spheres at four contact points. At the contact points, the contact surface is enlarged by plane sections of the respective sphere. A circular recess is created in each case, which connects the cavities and enables the removal of loose powder.

Table 2: Characteristics of the investigated core structures HDP, framework, and honeycomb.

name	HDP	FW	HC
			
wall thickness	0.20 mm	0.25 mm	0.18 mm
height	3.46 mm	2.48 mm	3.64 mm
sheet/core ratio	3.52	5.83	7.18

Before the manufacturing of the hybrid sandwich sheets, a mounting system is developed to ensure the successful realization of the manufacturing process. To achieve high part quality as well as to ensure the necessary process stability, the inserted sheet must be fixed plane and stable. As already mentioned above, sheet thicknesses of less than 1 mm are reasonable in the context of lightweight design. To realize these requirements (high process stability, low sheet thickness), a mounting system capable of generating a sufficient negative force in the z-direction without a form-locking connection is necessary. Consequently, a vacuum mounting system was selected as the most suitable concept, and hereafter described in detail.

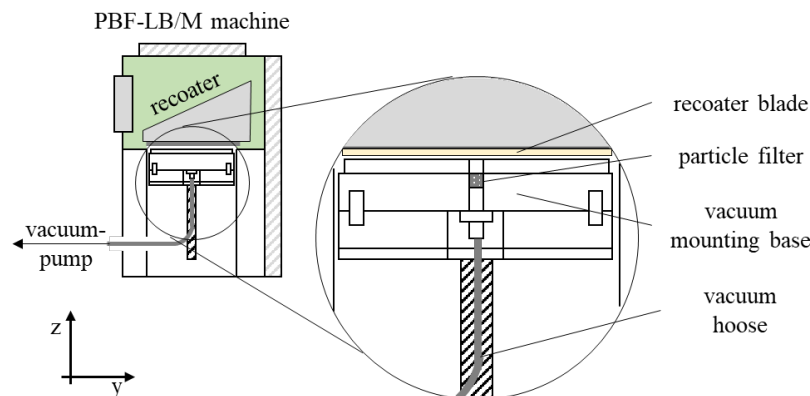


Figure 1: Schematic illustration of the vacuum mounting system integrated into an eos M270 PBF-LB/M system

A schematic illustration of the main components of the mounting system is shown in Figure 1. The system is designed for integration into the EOS M270 PBF-LB/M machine. The vacuum mounting base is located within the building chamber and is connected to the platform's lifting table through an adapter panel. Metal sheets with dimensions up to 200 mm x 200 mm can be mounted. A nozzle on the bottom of the vacuum mounting base provides a closed connection to the vacuum hose. The hose itself is led out of the system via a service tunnel, which is intended for the wiring of the conventional heating unit. At the other end of the vacuum hose, the vacuum pump is connected via a reducing adapter. The system has a total of three different filter units. To protect the pump from powder particles that may be sucked in from the building chamber, there is a filter unit at both ends of the hose system, after the vacuum plate and before the pump. The vacuum pump used is the model E2M1.5 from Edwards Ltd. UK which is designed for continuous operation. The motor power is 0.16 kW at a constant speed of 2800 rpm with a suction volume of 1.8 m³/h and an ultimate pressure of 0.003 mbar. The required mounting area can be defined by the appropriate sealing cord (diameter 2.5 mm).

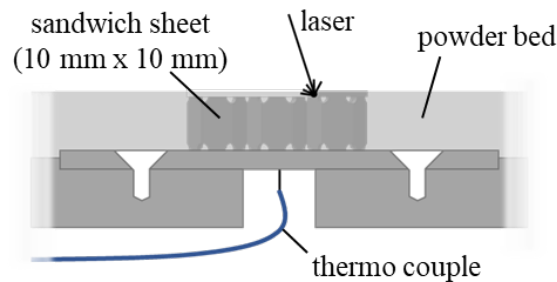


Figure 2: Set-up for in-situ temperature measurements. A detailed description of the setup can be found in [20].

To clarify the influence of the different process parameters on the thermally induced deformation of the rolled sheet, an in-situ temperature measurement was performed. The setup used allowed an estimation of the thermal history in the rolled sheet and can thus provide information on the associated thermal stresses.

The basic setup of the measuring system is shown in Figure 2. A detailed description of the setup is presented in [20]. Here, a C45 steel substrate plate of 220 mm x 220 mm was fixed on an adapter ring with minimal contact area. The base plate used has a recess, so that wiring for the thermocouple can be led from below the substrate plate through the shaft of the building platform. As shown, the thermocouple was spot welded directly onto the disc, ensuring maximum resolution through minimum tare volume, and thus minimal thermal inertia. A Testo 635 device with an accuracy of 0.3 °C was used to read out the data.

Results

The main challenge facing the manufacturing of hybrid sandwich sheets is to ensure a stable additive build-up with sufficient part densities.

First, the presented part geometries (HDP, FW, and HC) were built with the Ref parameter set. All investigated core structures could be successfully built at an edge length of 35 mm x 35 mm (Figure 3a-c). When increasing one edge length of the core structure to 105 mm, the vacuum collapsed for all geometries. Resulting in a collision of the recoater blade and the part due to excessive thermal-induced deformation of the sheet. In contrast to the Ref parameter set, the utilization of the Ev- parameter set led to a complete build-up of the HC geometry (Figure 3d-f).

Since only the HC structure could be built up, the core-to-sheet ratio could have a decisive role as an increased sheet/core ratio is favourable for reduced temperature input, but it might promote heat accumulation within the upper cover sheet due to insufficient heat dissipation. As the investigations of Khobzi et al. [21] also demonstrated in a comparable setting.

Nevertheless, even after a successful build-up, superelevations could be detected on one edge (Figure 3e). All other geometries (HDP, FW) considered could not be build-up either. However, upon removal of the sheet from the build chamber, severe distortion of the sheet along the y-axis was evident (Figure 3f). This distortion was compensated during build-up by the vacuum force applied in the opposite direction.

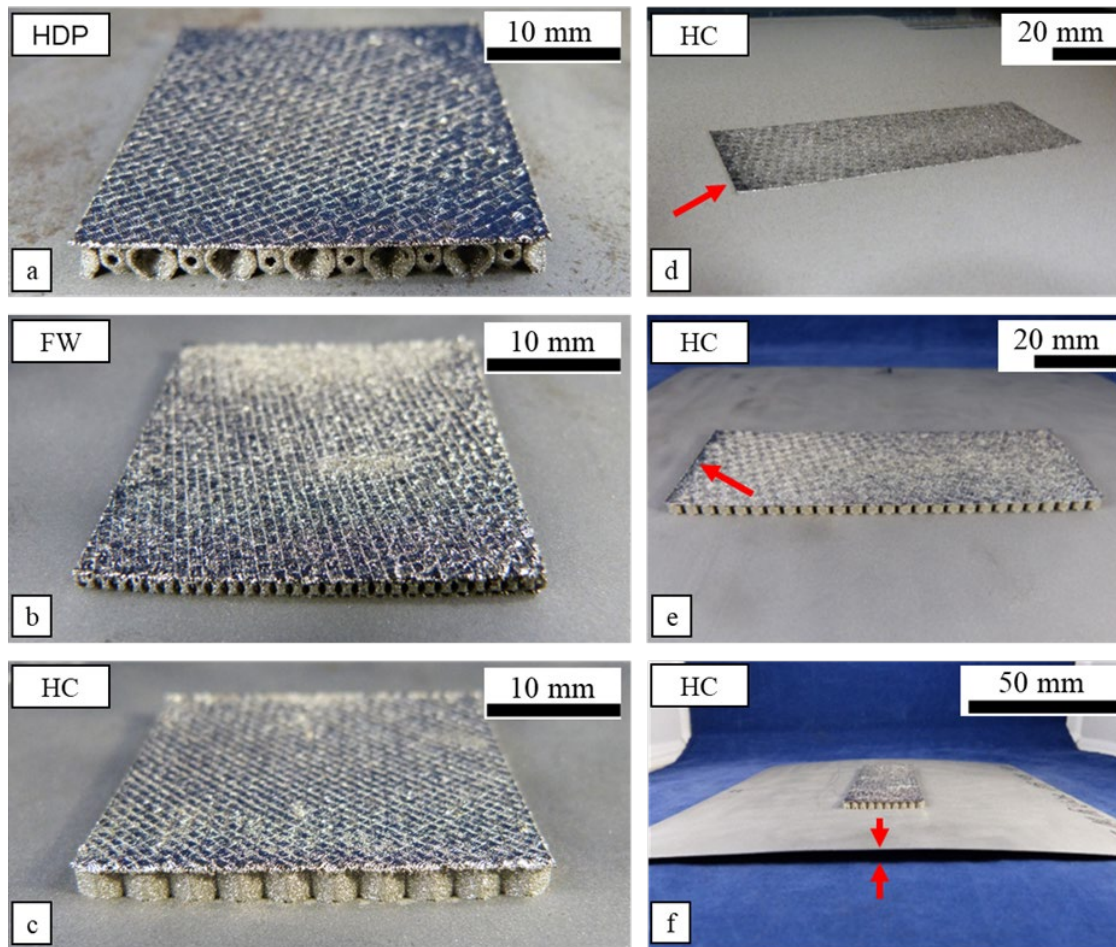


Figure 3: Built-up hybrid sandwich sheet with an edge length of 35 mm x 35 mm (a-c) and 105 mm x 35 mm (d-f). Note the geometry identification in the upper left corner. d) after the build-up inside the machine, the red arrow indicates superelevations. e) full build-up hybrid sandwich sheet, the red arrow indicates superelevated edge. f) Thermal-induced deformation of the rolled sheet after the build-up, depicted by red arrows.

To verify reproducibility, a total of three processes were carried out with the Ev- parameter set. After the successful build-up of the HC structure with an area of 105 x 35 mm², the resulting geometrical deviation was measured and is depicted in Figure 4. Due to the symmetry of the hybrid sandwich sheet, the ROI for the measurement of the geometric deviation is reduced to an area of about 100 mm x 15 mm to reduce the number of measuring points. The upper graph in figure 4 describes the deviation in the x-z plane, and the lower graph the deviation in the x-y plane. In the lower graph (x-y plane), the deviation of the entire area is represented by a coloured scale. In the upper graph, three y-positions were selected and compared.

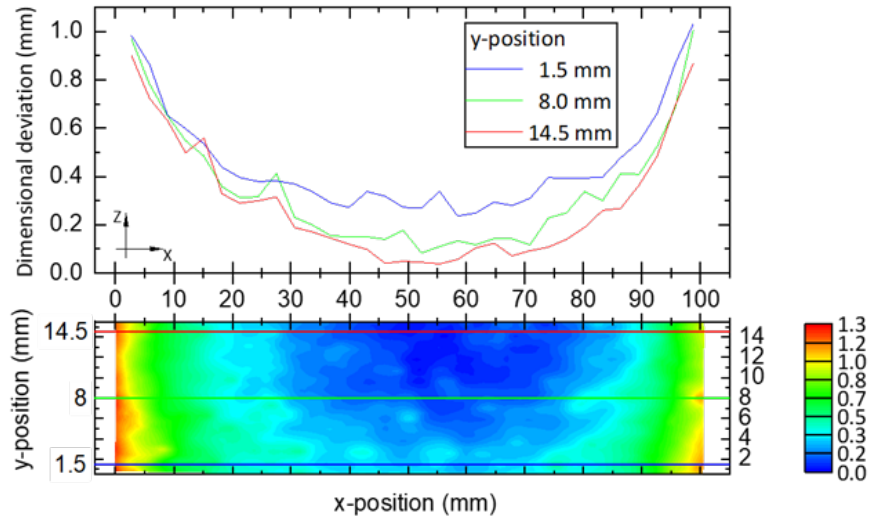


Figure 4: Illustration of the geometric deviation of the hybrid sandwich sheet built. Due to the symmetry of the part, the measurement was carried out on half (100 mm x 15 mm) of the sheet. Representation of the partial surface in the x-y plane in the lower graph.

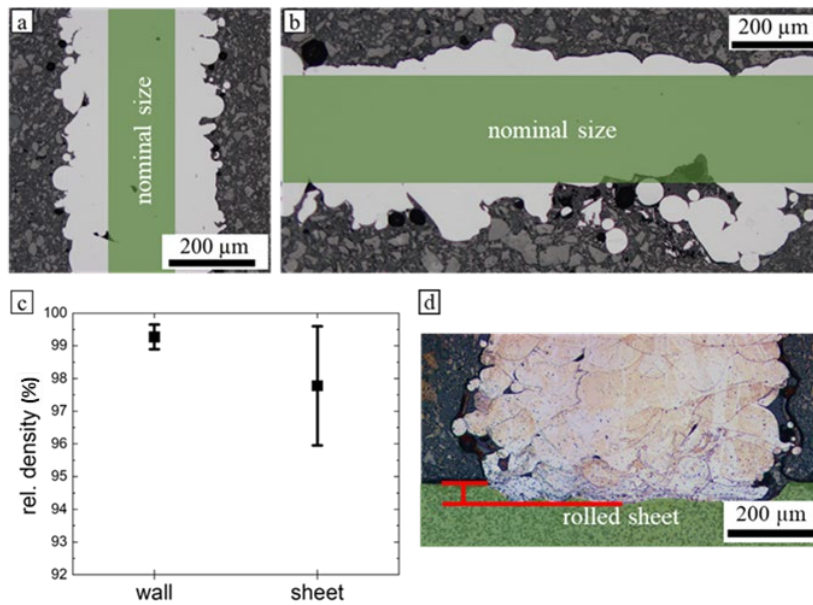


Figure 5: Micrographs and density analysis of the hybrid sandwich sheet. An exemplary illustration of the wall geometries with depicted nominal size in green (a), the cover sheet with depicted nominal size in green (b) and the resulting relative densities (c). (d) Etched wall geometry with the resulting penetration depth marked in red.

Both graphs indicate a positive deviation from the nominal geometry at the outer edges of the sheet. This is comparable to the results in [16] for other materials. The maximum global deviation is about 1 mm and decreases towards the centre of the part to a minimum of 0.05 mm. With a layer thickness of 0.04 mm, this corresponds to 25 layers.

It should be noted that the geometric deviation during the build-up is likely to be much smaller due to the applied vacuum force, which counteracts the induced deformation of the sheet. However, it was shown before that the parameter sets had a significant influence on the build-

up result and even for the successful build-up with reduced energy comparably high dimensional deviations in a range of multiple layers occur.

Figure 5 shows the micrographs and the corresponding relative densities of the build-up hybrid sandwich sheets. As depicted in Figure 5c, the relative density of the vertical walls is 99.27 %. An example of the wall quality is shown in Figure 5a. The edge contours are marked by process-typical sintering [22]. In addition, single Lack-of-Fusion defects are recognizable in the micrograph. The width of the walls is significantly wider than the nominal geometry width (0.18 mm). In addition to the surface sintering of powder particles, this may be attributable to the reduced scanning speed of the Ev- parameter, since a reduced scanning speed tends to cause a wider melt pool [23]. Nevertheless, some Lack-of-Fusion defects are still recognizable, which can be attributed to the reduced energy input [24]. The density analysis of the upper cover sheet reveals a strong geometrical deviation and, in addition, a clear expression of surface sintering in combination with a large number of defects (Figure 5b). The significant amount of non-supported exposure area, especially during the build-up of the first cover sheet layer, led to a severe expression of surface sintering, and a predominantly uneven surface. Overall, this leads to a relative density of 97.78 % with a comparatively high standard deviation of 1.8 %. Nevertheless, the thickness of the build-up sheet (about 330 μm) is approximately in the range of the STL model of 0.3 mm.

To evaluate the penetration depth of the laser and thus the quality of the metallurgical bonding between the rolled sheet and the additive structure, the etched wall geometry is shown in Figure 5d. Using the EV- parameter with 49.6 J/mm^3 at 125 W laser power, the penetration depth is in the range of 50 μm . Schaub et al. [7] illustrated a penetration depth of 223 μm for a comparable volume energy density but a significantly higher laser power, 46 J/mm^3 respectively 250 W. In the same publication, they also investigated a comparable laser power of 100 W resulting in a penetration depth of 27 μm . In this context, the penetration depth of about 50 μm measured in this study is within a comparable range, which illustrates the dominant influence of the laser power.

As the results of the build-up revealed, most of the process failures occurred when the upper cover sheet was reached. Only the HC core structure could be successfully built using the Ev-parameter. Consequently, the geometrical characteristics of the considered core structures seem to be crucial. Here, the core geometries differ in the varying contact areas of the core and the upper cover sheet. The difference in the sheet/core area ratio (table 2) is thereby most significant between the HDP and the HC structure. In addition, [25–27] have shown that geometric features such as overhangs and the associated amount of energy directed into the loose powder influence the part temperature. A different temperature can in turn affect the deformations occurring in the rolled sheet [28]. To consider the influence of the geometry on the resulting deformations, an in-situ thermal analysis of the HC geometry (approx. 10 mm x 10 mm) was carried out using the setup introduced in [20] and [29].

The results of the in-situ thermal analysis are (exemplary for the HC structure) depicted in Figure 6. The investigated HC geometry is divided into four areas depending on the surface characteristics. The first section is characterized by an exponential increase in area. In the second section, the exposure area is constant at 30.21 mm^2 until the third section shows a reduction to the level of the initial layer (14.53 mm^2). The fourth sector describes the sudden increase from 14.53 mm^2 to 109.47 mm^2 in which the upper cover sheet is build-up. As the previous results have shown, this area is significant for a practicable process. Figure 6 shows the progression of the maxima for each layer relative to the initial temperature. Note that the number of measurement points for the Ev- parameter set is halved due to the doubled layer thickness compared to the Ref parameter. As shown, the depicted temperature maxima increase in the first sector parallel to the exposure area per layer. For the initial layer, the maximum

temperature difference of the Ref parameter is 7.2 K, and for the Ev- parameter set 5.4 K. Concerning the exposure area, these values are in good correspondence with the values in [20].

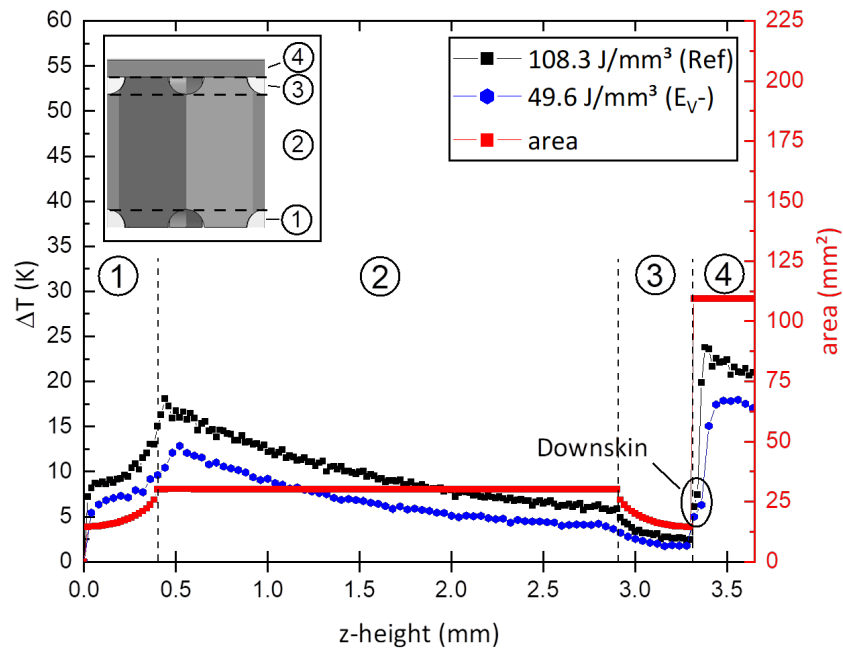


Figure 6: Illustration of the relative temperature and area progression over the z-height for the parameters Ref and Ev-. Note the doubled layer thickness of the Ev- parameter, resulting in a reduction of measurement points. The various significant regions of the built-up HC structure are plotted in the top left corner.

Both temperature maxima progressions increase exponentially up to a value of 18.06 K (Ref) and 12.84 K (Ev-) despite the increasing distance to the thermocouple. The maximum temperature difference is reached for the Ref parameter set at a z-height of 0.44 mm, respectively 0.02 mm (one layer) after reaching the z-height of the second sector (0.42 mm). For the Ev- parameter set, the highest temperature difference is present only at a z-height of 0.52 mm, thus 0.1 mm after reaching the height in the second sector. During the constant exposure area of 30.21 mm² in the second sector, the temperature differences of both parameter-sets decrease with increasing distance to the measuring position in the base plate to 5.97 K (Ref) and 3.22 K (Ev-). Due to the further successive reduction of the exposure area in the third sector to 14.46 mm², the temperature differences decline continuously. At the transition between the third and fourth sectors, there is a sudden increase in the exposure area in the sector of the upper cover sheet to 109.47 mm². In the first two layers of the upper cover sheet, downskin-parameters typical for the PBF-LB/M process and representing low energy input were used [30]. Despite the meanwhile progressed distance to the measuring position, the temperature differences resulting from the downskin-parameters can also be identified in the graph. The parameter sets Ref and Ev- used from the third layer within the fourth sector lead to a maximum temperature difference of 23.8 K (Ref) and 18.0 K (Ev-), respectively. By the time the part is finished, the temperature differences decrease again.

Based on the results, it can be deduced that the reduced temperature level during the Ev- build-up, leads to a reduction in deformation as [28] and [31] highlighted the importance of the temperature level on the resulting deformations.

Conclusion

As the results of the build-up of the three different core structures and the in-situ temperature measurement of the HC structure revealed, the geometry of the sandwich sheet and

the exposure parameters used influence the resulting temperatures and thus the forces to be compensated by the vacuum mounting system. By choosing a suitable parameter combination with reduced energy, the heat input into the rolled sheet is reduced and at the same time, heat accumulation in the upper cover sheet is avoided. These results are in strict contrast to the conventional PBF-LB/M manufacturing strategies, which aim at a targeted and fast transport of the heat, especially in areas with a significant overhang [32]. The high amount of overhangs of the sandwich sheets is beneficial within the production concept presented for the manufacturing of hybrid sandwich sheets, as these overhangs protect the rolled sheet inherently from excessive thermal energy input and thus from deformation. Within further investigations, especially the influence of different core geometries should be examined by numerical studies. This would allow a critical sheet-to-core ratio to be determined, which in turn could be used as a design parameter in the future development of hybrid sandwich sheets.

Acknowledgement

This work was kindly supported by the German Research Foundation (DFG) under project numbers WI 2118/9-3 and WI 2118/17-1. Furthermore, we would like to thank Prof. A. Erman Tekkaya and Dr. Stephan Rosenthal from the Institute of Forming Technology and Lightweight Components at the TU Dortmund for providing the CAD files of the core structures. We also thank Fabian Schulz for the execution of the manufacturing processes within his bachelor thesis.

References

- [1] Wohlers T, Campbell RI, Diegel O, Kowen J, Mostow N, Fidan I. Wohlers report 2022: 3D printing and additive manufacturing global state of the industry. Fort Collins, Colo., Washington, DC: Wohlers Associates; ASTM International; 2022.
- [2] Yin S, Yan X, Chen C, Jenkins R, Liu M, Lupoi R. Hybrid additive manufacturing of Al-Ti6Al4V functionally graded materials with selective laser melting and cold spraying. *Journal of Materials Processing Technology* 2018;255:650–5. <https://doi.org/10.1016/j.jmatprotec.2018.01.015>.
- [3] Tan C, Zhou K, Ma W, Min L. Interfacial characteristic and mechanical performance of maraging steel-copper functional bimetal produced by selective laser melting based hybrid manufacture. *Materials & Design* 2018;155:77–85. <https://doi.org/10.1016/j.matdes.2018.05.064>.
- [4] Merklein M, Junker D, Schaub A, Neubauer F. Hybrid Additive Manufacturing Technologies – An Analysis Regarding Potentials and Applications. *Physics Procedia* 2016;83:549–59. <https://doi.org/10.1016/j.phpro.2016.08.057>.
- [5] Ahuja B, Schaub A, Karg M, Schmidt R, Merklein M, Schmidt M. High power laser beam melting of Ti 6 Al 4 V on formed sheet metal to achieve hybrid structures. In: Helvajian H, Piqué A, Wegener M, Gu B, editors. *Laser 3D Manufacturing II*. SPIE; 2015, 93530X.
- [6] Merklein M, Schulte R, Papke T. An innovative process combination of additive manufacturing and sheet bulk metal forming for manufacturing a functional hybrid part. *Journal of Materials Processing Technology* 2021;291:117032. <https://doi.org/10.1016/j.jmatprotec.2020.117032>.
- [7] Schaub A, Ahuja B, Butzhammer L, Osterziel J, Schmidt M, Merklein M. Additive Manufacturing of Functional Elements on Sheet Metal. *Physics Procedia* 2016;83:797–807. <https://doi.org/10.1016/j.phpro.2016.08.082>.
- [8] Schaub A, Juechter V, Singer RF, Merklein M. Characterization of Hybrid Components Consisting of SEBM Additive Structures and Sheet Metal of Alloy Ti-6Al-4V. *KEM* 2014;611-612:609–14. <https://doi.org/10.4028/www.scientific.net/KEM.611-612.609>.

- [9] Rosenthal S, Hahn M, Tekkaya AE, Platt S, Kleszczynski S, Witt G. Speeding up Additive Manufacturing by Means of Forming for Sheet Components with Core Structures. *Int. J. of Precis. Eng. and Manuf.-Green Tech.* 2021. <https://doi.org/10.1007/s40684-021-00384-x>.
- [10] Gruber K, Dziedzic R, Kuźnicka B, Madejski B, Malicki M. Impact of high temperature stress relieving on final properties of Inconel 718 processed by laser powder bed fusion. *Materials Science and Engineering A* 2021;813:141111. <https://doi.org/10.1016/j.msea.2021.141111>.
- [11] Promopattum P, Yao S-C. Influence of scanning length and energy input on residual stress reduction in metal additive manufacturing: Numerical and experimental studies. *Journal of Manufacturing Processes* 2020;49:247–59. <https://doi.org/10.1016/j.jmapro.2019.11.020>.
- [12] Ali H, Ghadbeigi H, Mumtaz K. Effect of scanning strategies on residual stress and mechanical properties of Selective Laser Melted Ti6Al4V. *Materials Science and Engineering A* 2018;712:175–87. <https://doi.org/10.1016/j.msea.2017.11.103>.
- [13] Simson T, Emmel A, Dwars A, Böhm J. Residual stress measurements on AISI 316L samples manufactured by selective laser melting. *Additive Manufacturing* 2017;17:183–9. <https://doi.org/10.1016/j.addma.2017.07.007>.
- [14] Mugwagwa L, Dimitrov D, Matope S, Yadroitsev I. Influence of process parameters on residual stress related distortions in selective laser melting. *Procedia Manufacturing* 2018;21:92–9. <https://doi.org/10.1016/j.promfg.2018.02.099>.
- [15] Levkulich NC, Semiatin SL, Gockel JE, Middendorf JR, DeWald AT, Klingbeil NW. The effect of process parameters on residual stress evolution and distortion in the laser powder bed fusion of Ti-6Al-4V. *Additive Manufacturing* 2019;28:475–84. <https://doi.org/10.1016/j.addma.2019.05.015>.
- [16] Magana-Carranza R, Sutcliffe CJ, Patterson EA. The effect of processing parameters and material properties on residual forces induced in Laser Powder Bed Fusion (L-PBF). *Additive Manufacturing* 2021;46:102192. <https://doi.org/10.1016/j.addma.2021.102192>.
- [17] Sabooni S, Chabok A, Feng SC, Blaauw H, Pijper TC, Yang HJ et al. Laser powder bed fusion of 17–4 PH stainless steel: A comparative study on the effect of heat treatment on the microstructure evolution and mechanical properties. *Additive Manufacturing* 2021;46:102176. <https://doi.org/10.1016/j.addma.2021.102176>.
- [18] Rashid R, Masood SH, Ruan D, Palanisamy S, Rahman Rashid RA, Brandt M. Effect of scan strategy on density and metallurgical properties of 17-4PH parts printed by Selective Laser Melting (SLM). *Journal of Materials Processing Technology* 2017;249:502–11. <https://doi.org/10.1016/j.jmatprotec.2017.06.023>.
- [19] Platt S, Wegner J, Kleszczynski S, Witt G. Effect of scan strategy, re-melting and exposure time on the microstructure of stainless steel 17 - 4 PH fabricated by laser powder bed fusion of metals. In: *International Conference on Additive Technologies*, p. 85–91.
- [20] Schnell N, Sievert M, Kleszczynski S, Witt G, Ploshikhin V. Alternative approach on an in-situ analysis of the thermal progression during the LPBF-M process using welded thermocouples embedded into the substrate plate. *SFF Symposium* 2019;2019(30):1264–80.
- [21] Khobzi A, Farhang Mehr F, Cockcroft S, Maijer D, Sing SL, Yeong WY. The role of block-type support structure design on the thermal field and deformation in components

- fabricated by Laser Powder Bed Fusion. *Additive Manufacturing* 2022;51:102644.
<https://doi.org/10.1016/j.addma.2022.102644>.
- [22] Shange M, Yadroitsava I, Du Plessis A, Yadroitsev I. Roughness and Near-Surface Porosity of Unsupported Overhangs Produced by High-Speed Laser Powder Bed Fusion. *3D Printing and Additive Manufacturing* 2022;9(4):288–300.
<https://doi.org/10.1089/3dp.2020.0097>.
- [23] Keshavarzkermani A, Marzbanrad E, Esmaeilzadeh R, Mahmoodkhani Y, Ali U, Enrique P d. et al. An investigation into the effect of process parameters on melt pool geometry, cell spacing, and grain refinement during laser powder bed fusion. *Optics & Laser Technology* 2019;116:83–91. <https://doi.org/10.1016/j.optlastec.2019.03.012>.
- [24] Liu W, Chen C, Shuai S, Zhao R, Liu L, Wang X et al. Study of pore defect and mechanical properties in selective laser melted Ti6Al4V alloy based on X-ray computed tomography. *Materials Science and Engineering A* 2020;797:139981.
<https://doi.org/10.1016/j.msea.2020.139981>.
- [25] Wei LC, Ehrlich LE, Powell-Palm MJ, Montgomery C, Beuth J, Malen JA. Thermal conductivity of metal powders for powder bed additive manufacturing. *Additive Manufacturing* 2018;21:201–8. <https://doi.org/10.1016/j.addma.2018.02.002>.
- [26] Cheng B, Lane B, Whiting J, Chou K. A Combined Experimental-Numerical Method to Evaluate Powder Thermal Properties in Laser Powder Bed Fusion. *J. Manuf. Sci. Eng* 2018;140(11). <https://doi.org/10.1115/1.4040877>.
- [27] Wegner J, Best JP, Schnell N, Kleszczynski S. Structural deviations of bulk metallic glasses in downfacing surfaces fabricated via Laser Powder Bed Fusion. *Procedia CIRP* 2022;111:105–10. <https://doi.org/10.1016/j.procir.2022.08.147>.
- [28] Mirkoohi E, Dobbs JR, Liang SY. Analytical mechanics modeling of in-process thermal stress distribution in metal additive manufacturing. *Journal of Manufacturing Processes* 2020;58:41–54. <https://doi.org/10.1016/j.jmapro.2020.08.009>.
- [29] Schnell N, Schoeler M, Witt G, Kleszczynski S. Experimental and numerical thermal analysis of the laser powder bed fusion process using in situ temperature measurements of geometric primitives. *Materials & Design* 2021;209:109946.
<https://doi.org/10.1016/j.matdes.2021.109946>.
- [30] Khan HM, Dirikolu MH, Koç E. Parameters optimization for horizontally built circular profiles: Numerical and experimental investigation. *Optik* 2018;174:521–9.
<https://doi.org/10.1016/j.ijleo.2018.08.095>.
- [31] Mukherjee T, Zhang W, DebRoy T. An improved prediction of residual stresses and distortion in additive manufacturing. *Computational Materials Science* 2017;126:360–72.
<https://doi.org/10.1016/j.commatsci.2016.10.003>.
- [32] Rombouts M, Kruth JP, Froyen L, Mercelis P. Fundamentals of Selective Laser Melting of alloyed steel powders. *CIRP Annals - Manufacturing Technology* 2006;55(1):187–92.
[https://doi.org/10.1016/S0007-8506\(07\)60395-3](https://doi.org/10.1016/S0007-8506(07)60395-3).